Dependence of Adhesion on Degradation Mechanisms of Ethylene Co-Vinyl Acetate Encapsulants Over the Lifetime of Photovoltaic Modules

Patrick Thornton[a], Stephanie L. Moffitt[b], Laura T. Schelhas[b,1], Reinhold H. Dauskardt[a]

[a] Department of Materials Science and Engineering, Stanford University, Stanford, CA, 94305, USA
[b] Applied Energy Division, SLAC National Accelerator Laboratory, Menlo Park, CA, 94025, USA
[1] (Present Address) National Renewable Energy Laboratory, 15013 Denver West Pkwy., Golden, CO, 80401, USA

Corresponding Author – Reinhold H Dauskardt (rhd@stanford.edu)

Abstract:

The long-term reliability of encapsulation has a critical impact on the overall cost and effectiveness of photovoltaic modules. An often overlooked but important element of this reliability concerns adhesive degradation of the encapsulant, which results in delamination. This work critically examines the degradation mechanisms – deacetylation, β-scission, and hydrolytic depolymerization – primarily responsible for adhesion loss in ethylene co-vinyl acetate (EVA) encapsulants to provide evidence and clarity regarding the contribution of these mechanisms to the adhesive degradation over the lifetime of a module. EVA samples obtained from mini-modules exposed in two sets of controlled, accelerated conditions – with and without ultraviolet (UV) radiation – are characterized to find specific evidence for the proposed degradation mechanisms. The mini-modules were exposed up to 10,000 hours, which represents up to 15-20 years in the field. Results affirm that initially, deacetylation dominates the degradation before scission takes over, followed by hydrolytic depolymerization. Additional analysis highlights the climacteric interdependency between deacetylation and hydrolytic depolymerization as it relates to eventual delamination, where deacetylation products catalyze interfacial hydrolysis reactions. Furthermore, effects occurring at a given interface are isolated, explicitly providing evidence for how these mechanisms are nonuniform throughout the thickness of the EVA. Results demonstrate that the EVA that interfaces with the glass as opposed to the cell experiences increased levels of degradation, explaining why this initially stronger interface becomes the preferential interface for delamination after longer periods of exposure. Additionally, elevated temperatures alone are shown to induce limited migration of sodium ions across the glass/EVA interface.

Keywords: EVA; photovoltaic encapsulation; interface delamination; polymer degradation; adhesion; reliability

1. Introduction

Encapsulation serves a critical purpose in extending the life and protecting photovoltaic (PV) modules. While new polymers have been explored, ethylene co-vinyl acetate (EVA) remains the primary low-cost encapsulation material used for c-Si PV modules with a combination of desirable properties, including high transparency, optical coupling, and adhesion along with providing physical and electrical isolation of the solar cells and circuit components [1,2]. The degradation and failure of the encapsulant within the module structure, specifically loss of adhesion and delamination from adjacent materials, diminish the useful lifetime of PV modules [3].

The degradation of EVA has been investigated and degradation pathways are generally known [4–11], including in solar modules [12–15], although understanding of the effects of surrounding constraints (i.e. laminated within a solar module) is often lacking. Another limitation involves the shorter exposure times and the resulting uncertainties in long-term effects [6,13]. With the development of a novel adhesion metrology [16,17], a recent adhesion reliability study has revealed that replicating decade-long degradation processes requires accelerated aging exposure times much longer than those generally used [18]. Furthermore, the reliability model developed within that study [18], which was based on polymer degradation reactions and accelerated indoor and field exposures, revealed the most relevant degradation pathways in EVA solar encapsulants – specifically, deacetylation, β-scission, and hydrolytic depolymerization or interface hydrolysis (**Figure 1**).

Deacetylation attacks the vinyl acetate moieties of the EVA, resulting in the production of byproducts like acetic acid; β-scission attacks the carbon backbone, resulting in a reduction in molar mass and alteration of thermomechanical properties, and hydrolytic depolymerization breaks down the siloxane bonds at the glass/EVA and EVA/cell interfaces. These individual mechanisms dominate the overall loss of adhesive strength during different stages of the lifetime of the module. The model is modular and flexible and was shown to have predictive capability for the loss of adhesion in fielded modules ranging from 6 months to 30 years of exposure.

In this work we employ detailed characterization to reveal the critical interdependency between deacetylation and hydrolytic depolymerization reactions and their contribution to degradation. Using differential scanning calorimetry (DSC), small- and wide-angle X-ray scattering

(SAXS/WAXS) along with infrared and X-ray photoelectron spectroscopies (FTIR/XPS), we provide evidence that describes the evolution of the relevant degradation mechanisms throughout 10,000 hours of accelerated testing, confirming at which stages of exposure each mechanism dominates the overall degradation. Additionally, we characterize the specific degradation occurring at the encapsulant interfaces within fully constructed mini-modules instead of simply within freestanding films or bulk EVA – something that is generally absent in previous studies – which enables more accurate results and correlations with field degradation. This yields compelling evidence that helps explain why the glass/EVA interface eventually becomes the weaker interface [18,19] and expands our understanding of how EVA adhesively degrades, providing a more comprehensive explanation for delamination that affects solar modules worldwide.

2. Methods and Materials

2.1 Sample Preparation

EVA (33% vinyl acetate by mass, 14% molar, PhotoCap 15585P UF/HLT, Specialized Technology Resources, Inc.) was taken from single-cell (150 mm x 150 mm) photovoltaic mini-modules that had been exposed to two sets of accelerated aging conditions: ‘light’ – 65˚C and 30% relative humidity (RH) under 340 nm UV light (Atlas Ci4000 Weather-Ometer®, 81 W/m^2, ~1.4x UV suns), and ‘dark’ – 85˚C and 13.5% RH without UV light (Blue M, Model AC-7620HB chamber). The ‘light’ condition parameters were selected to compensate for heating effects from the UV light, allowing for accurate comparisons between the two sets of conditions. Samples had been aged for up to 10,000 hours, which for ‘light’ conditions roughly equates to 15-20 years in the field. This comparison assumes a fixed plate field configuration that receives about .25 UV suns on average, which is a typical value for the United States, and an acceleration of 1.4x for every 10˚C above an average effective module temperature of ~55˚C. Sections of EVA were mechanically removed from between the cell and the 3 mm borosilicate front glass. The weaker interface was separated through adhesion testing, which utilized width-tapered cantilever beam tests [16,17]. The EVA was then mechanically peeled from the remaining interface, providing a freestanding film for testing and analysis.

2.2 Differential Scanning Calorimetry (DSC)

DSC (TA Instrument Q2000) was employed to ascertain the percent crystallinity (χ_c) in the EVA. The conditions for the measurement of the heat flow are as follows: 2 heating and cooling cycles conducted from -40˚C to 150˚C at a rate of 10˚C per minute and a 5-minute dwell period at the minimum and maximum temperature for each cycle. The integrated area beneath the endothermic peak of the second heating cycle (the enthalpy of fusion, ΔH_f) was calculated and utilized in the χ_c computation. The integration limits were positioned around the primary melting peak(s) (~50˚C-80˚C), and a sigmoidal baseline was used. The second heating cycle was chosen to explore crystallinity because the specific thermal history is expunged from the EVA during the first heating cycle, allowing for a more accurate comparison of material-specific, microstructural features. To evaluate χ_c, ΔH_f was normalized against the enthalpy of fusion for 100% crystalline polyethylene, ΔH_f^{PE} (277 J/g) (see Eqn. 1). This normalization procedure is typical for polyethylene-based polymers as it utilizes a common reference point for more accurate and universal comparisons.

$$\chi_c = \frac{\Delta H_f}{\Delta H_f^{PE}} \times 100 \tag{1}$$

2.3 Wide-Angle X-ray Scattering (WAXS)

WAXS experiments were conducted on beamline 11-3 at the Stanford Synchrotron Radiation Lightsource (SSRL) at the SLAC National Accelerator Laboratory. Data were obtained from testing in both transmission (t-WAXS) and grazing-incidence (GIWAXS) geometries with an X-ray photon energy of 12.7 keV. Sample-to-detector distances were nominally 200 mm and were calibrated with LaB_6. For GIWAXS, the X-ray beam incident angle was 6˚. The data were collected with a Rayonix MX225 detector and integrated using the GSASII software package [20].

2.4 Small-Angle X-ray Scattering (SAXS)

SAXS experiments were conducted on beamline 1-5 at SSRL at the SLAC National Accelerator Laboratory. Data were obtained from testing in both transmission and grazing-incidence geometries. For SAXS performed in transmission (t-SAXS) and grazing-incidence (GISAXS), the sample-to-detector distance was 2904 and 2860 mm, respectively (as calibrated using a silver behenate standard). For GISAXS, the X-ray beam incident angle was 3˚. The X-ray photon energy was 12 keV (1.033 Å) for both, and a Rayonix 165 SX CCD area detector collected the scattering patterns. Two dimensional SAXS data were integrated in IgorPro utilizing the Nika software package [21].

2.5 Fourier Transform Infrared Spectroscopy – Attenuated Total Reflectance (FTIR-ATR)

FTIR-ATR (Nicolet iS50) was employed to understand the chemical changes occurring within the EVA. Attenuated Total Reflectance (ATR) mode enabled a focused exploration of the interfacial chemistry. Background IR spectra were collected approximately every 30 minutes to enable accurate background subtraction with 16 scans collected and averaged at a resolution of 4 cm^{-1}. Sample IR spectra were averaged over 32 scans at the same resolution. Each spectrum was baselined in the Omnic® software utilizing the same 8 points for consistency. Following baseline subtraction, the spectra were normalized by the height of the 1466 cm^{-1} peak. 3 different locations on each section of EVA film were tested and analyzed. Their average and standard deviation constitute the data points and error bars, respectively, exhibited on the accompanying figures.

2.6 X-ray Photoelectron Spectroscopy (XPS)

Elemental surface analysis was conducted using XPS (PHI VersaProbe 3). Both sides of the EVA, where it interfaced with the glass and the cell, were surveyed from 0-1100 eV with a 1487 eV Al K_{α} X-ray radiation source. A neutralizer was employed to prevent charging of the sample. Survey scans were performed to reveal the presence and relative amounts of elemental constituents at the relevant interfaces after aging. 3 unique locations for each sample were tested. The data points and error bars are constructed using the averages and standard deviations, respectively. Elements found to be consistently below 0.5% of the composition were ignored since their contribution could not be distinguished from noise.

3. Results and Discussion

3.1 Bulk Crystalline Regions

EVA utilized as solar encapsulants generally has between 28-33% vinyl acetate (VA) by weight, making it a semi-crystalline polymer. Results from DSC, showing EVA crystallinity as a function of exposure time are shown in **Figure 2**. Under 'light' conditions, over the first 1000 hours, the crystallinity increases by 5%. However, between 2000 and 5000 hours, the crystallinity drops by ~18%. Samples aged in 'dark' conditions mildly follow a similar trend with a slight increase over the first 2000 hours and an ~8% drop over the subsequent 3000 hours. Over the final 5000 hours, the percent crystallinity remains steady in both cases.

GIWAXS and t-WAXS results are shown in **Figure 3a** and **Figure 3b**, respectively, with scattering intensity as a function of the scattering vector, Q. The primary EVA peaks are visible and labeled at 1.39 $Å^{-1}$, 1.49 $Å^{-1}$, and 1.63 $Å^{-1}$, correlating respectively with the [001] monoclinic crystalline phase (MCP) peak, the [110] orthorhombic crystalline phase (OCP) peak, and the [200] peak shared by both phases. In **Figure 3a** (GIWAXS), the 10,000 hour 'light' sample has apparent magnitude increases for both the [001] and [200] shoulders relative to the height of the primary orthorhombic peak. However, in **Figure 3b** (t-WAXS), after normalizing by thickness, similar magnitude changes are not seen between samples aged for 10,000 hours in 'dark' and 'light' conditions. Note that GIWAXS data have been normalized by the [110] OCP peak to allow for a qualitative comparison since quantitative comparison on rough samples is unreliable in GIWAXS geometry. This relative increase in magnitude of the [001] and [200] shoulders likely results from a correlative increase in MCP compared to OCP. This conclusion is further substantiated by noting that the [200] shoulder also increases but by a lesser amount, which would be expected since both phases contribute to this peak. Thus, the sample aged in 'light' conditions has a higher MCP to OCP ratio after 10,000 hours of exposure.

Due to the geometry of how the incident X-rays interact with the material, GIWAXS probes the crystalline characteristics in both the in-plane and out-of-plane directions since the X-rays have components perpendicular to both axes. t-WAXS is primarily orthogonal to a singular axis and therefore, primarily probes in-plane crystallinity (see **Figure S2**), making out-of-plane contributions negligible. This helps elucidate the differences seen between t-WAXS and GIWAXS. Throughout exposure, the crystallographic changes seem to be primarily occurring in the out-of-plane direction since the differences are only observed through GIWAXS.

MCP crystallites are thinner crystallites that have been shown to form from shorter sequences of ethylene. This has been attributed to a thermodynamic favorability difference between the interior and the surface of EVA crystallites, with the surface favoring the parallel packing of MCP and the interior favoring OCP [22]. As crystallites become thinner and smaller, their surface area to volume ratio increases, which eventually allows for the MCP to dominate over the OCP. As shown here, an increase in the MCP to OCP ratio occurs after long-term aging in 'light' conditions. This increase can be understood by considering β-scission along the polyethylene backbone, which interrupts the packing sequence of the polyethylene, leading to thinner, MCP crystallites. Furthermore, UV-induced radicals are energetically necessary for β-scission, which explains why these crystallographic changes would not occur in 'dark' conditions. Thus, the WAXS results evidence the β-scission occurring in the crystalline regions.

Furthermore, deacetylation has been suggested to facilitate the crystallization process [23] and to be heavily UV driven [24]. The initial crystallinity increase shown in **Figure 2** for the 'light' conditions supports these conclusions. This relative increase in crystallinity is followed by an extensive decrease between 2000 and 5000 hours, suggesting a competition of effects, with deacetylation dominating initially and β-scission reactions dominating at intermediary time scales. This delayed dominance of β-scission aligns with the diffusion-limited oxidation evidence described by Schlothauer *et al.* [25] that suggests scission events would be delayed on account of the kinetics of oxygen diffusion through EVA. A considerable decrease in χ_c provides evidence for UV-driven chain scission. Successive chain scission reactions would limit the continuous polyethylene sequences and, thus, lower the overall crystallinity. The arrows above **Figure 2** denote the approximate time periods over which each degradation pathway (referenced by roman numerals with I, II, and III indicating deacetylation, β-scission, and hydrolytic depolymerization, respectively) dominates the overall degradation based on this DSC data. These regions align with those discussed by Tracy *et al.* [18] that were based on analysis of field-aged modules and subsequent sensitivity studies within the analytical degradation model. Our current analysis of accelerated lab-aged mini-modules provides compelling validation for their field-based conclusions and importantly provides additional context regarding when a transition from deacetylation to β-scission might be expected.

GISAXS (**Figure 3c**) and t-SAXS (**Figure 3d**) were conducted after a range of accelerated exposure periods, up to 10,000 hours, and results are shown with scattering intensity as a function of the scattering vector, Q. In both geometries, results indicate a long period spacing of ~13 nm that remains invariable throughout aging. This characteristic spacing indicates some periodicity and order in the spacing between amorphous and crystalline EVA regions. Thus, the long period ordering between amorphous and crystalline regions is generally unaffected by the aging. t-SAXS results primarily illuminate the characteristic spacing in-plane but not through the EVA thickness, whereas GISAXS results inform on both in-plane and out-of-plane features as explained in the WAXS discussion. The similarity between results suggests a level of isotropism for this feature.

3.2 Interfacial Chemistry

FTIR-ATR was utilized to investigate the chemical changes at the glass/EVA and EVA/cell interfaces. **Figure 4** includes several representative spectra from both 0 and 10,000 hours of accelerated exposure at both interfaces. **Figure 5** includes data from both interfaces after 0, 2000, and 10,000 hours. It conveys several critical trends at certain peaks of interest (located near 3500, 2920, 1560, and 1125 cm^{-1}). For **Figure 5a** and **Figure 5c**, results after aging are normalized to initial values at their respective interfaces (i.e. glass/EVA to glass/EVA). For **Figure 5d**, the results are all normalized to the initial EVA/cell interface for visual clarity.

The first region of interest, highlighted in **Figure 5a**, is the broad -OH stretch peak between 3115 and 3650 cm^{-1}. At the EVA/cell interface, absorbance levels remain negligible and fairly constant throughout 10,000 hours of exposure. However, at the glass/EVA interface, we see a ~5x increase. This is true for both 'dark' and 'light' samples, which suggests an essential interaction between the glass and the EVA, leading to a catalytic degradative effect. -OH stretching can potentially come from different sources; we narrow down the scope of likely explanations below.

It is well documented that acetic acid develops through the degradation and break down of EVA [5,26], and one could reasonably postulate that this OH- peak arises from the -COOH group of the acid. However, upon closer inspection, the -OH group for these acids is shifted several hundred wave numbers, usually centered around ~3000 [27,28]. Additionally, one would expect this peak at both interfaces if its source were acetic acid since it develops at the EVA/cell interface as well [29,30]. Based on possible chemical reactions in EVA and the peak's location, it can be assigned to the development of alcohols, particularly vinyl alcohol moieties, through hydrolysis reactions along the main chain. In strong support of this conclusion, Tang *et al.* [31] conducted a controlled, partial conversion of EVA to vinyl alcohol copolymers and obtained evidence of alcohol formations through the measurement of a broad absorbance band located around 3450 cm^{-1}. Furthermore, analysis done on FTIR spectra of hydrolyzed EVA copolymers by Koopmans *et al*. [32] utilized the development of this -OH absorption band as a measure for the percentage incorporation of vinyl alcohol in hydrolyzed EVA copolymers. These vinyl alcohol producing, hydrolysis reactions can occur through traditional deacetylation at the ester groups, potentially creating a disparity between levels of acetic acid at the two interfaces due to the increased presence of these reactions at the glass/EVA interface. Additionally, since oxygen gas diffuses through the backsheet and encapsulant, the reactions can occur at the main chain hydrogen atoms.

For additional evidence regarding this breakdown of EVA, particularly at this glass/EVA interface, the ~1125 cm^{-1} peak is more closely examined (**Figure 5b**). As EVA partially converts to vinyl alcohol copolymers, the ~1125 cm^{-1} peak shifts to higher values around 1128 cm^{-1} [31]. This shift is detected here at the glass/EVA interface, as shown in **Figure 5b**. While the trend generally follows that seen in **Figure 5a**, the peak shift results suggest that the magnitude and scope of these conversions may be greater in ‘light’ conditions since that peak shift is consistently more pronounced. Altogether, the degradation seen here provides additional evidence for deacetylation and other hydrolysis reactions, especially at the glass/EVA interface and in ‘light’ conditions.

The third region of interest is at ~2920 cm^{-1}, which is associated with CH absorption along the main EVA backbone. In **Figure 5c**, a divergent trend is captured where approximate peak areas at the EVA/cell interface increase between 5-10% after 10,000 hours of exposures, whereas for the glass/EVA interface, the areas decrease over the same time. These trends exist for both ‘light’ and ‘dark’ conditions with levels for the ‘light’ samples initially rising and exceeding the equivalent ‘dark’ samples after 2,000 hours but falling over the subsequent 8,000 hours. Relative increases and decreases in this peak are associated with the competitive crosslinking and chain scission reactions, respectively [24,33]. Additionally, increased surface accumulations of other compounds without characteristic CH bonds could also contribute to relative peak reductions. Of particular interest in this region are the divergent trends between the two interfaces.

At the EVA/cell interface, an overall increase in peak area is observed, suggesting crosslinking reactions tend to dominate over scission here, whereas at the glass/EVA interface, relative decreases in peak area are observed. Slightly greater losses are seen for both samples exposed in ‘light’ conditions after 2000 hours, indicating an ultimate dominance of scission over crosslinking when exposed to UV. Advanced chain scission would be expected within the EVA closer to the light source since β-scission is accelerated by UV radiation [24]. However, UV-driven β-scission is not the only reaction competing with crosslinking. The slight drop in peak intensity at the 'dark' sample's glass/EVA interface suggests that other reactions also affect molecular bonding along the main chain. Additionally, some crosslinking reactions, especially earlier in the exposure period, potentially arise from reactions at previously unreacted peroxides present after the initial lamination procedure [34,35]. Regardless, the divergent response in this region further highlights the degradative differences between the interfaces.

The fourth area lies within the fingerprint region between ~1500 and ~1650 cm^{-1}. In **Figure 4**, the emergence and extensive increase in peaks is apparent over this stretch of wavenumbers. Some of these peak increases closer to 1650 cm^{-1} likely arise from the stretching modes of C=C bonds formed through degradation reactions I and II (see Figure. 1). Around 1560 cm^{-1}, as shown in **Figure 5d**, the spectral absorption along the EVA/cell interface gradually increases until, at 10,000 hours, the maximum peak height is ~3-6x for both sets of conditions. Along the other interface, the maximum peak height is initially ~3x higher than the EVA/cell peak. Minimal changes occur during the first 2,000 hours, but then over the next 8,000 hours, the maximum peak height in 'dark' conditions increases to ~15x the initial EVA/cell level and in 'light' conditions, that peak height increases to nearly 40x. The origin of these peaks comes from acetate ions and salts.

Wang *et al.* [36] comprehensively investigated acetate ions and salts using FTIR in the context of stabilizing cerium ions for the deposition of thin films. Their work helps elucidate the nature of the peaks that develop in this study. Symmetric and antisymmetric CO stretching modes can be found around ~1415 and ~1570 cm^{-1}, respectively. At lower concentrations of acetate, relatively weak peaks exist around 1560 and 1577 cm^{-1}. For intermediate concentrations, the ~1560 cm^{-1} peak provides a strong signal, and for high concentrations, the ~1577 and ~1560 cm^{-1} bands merge and intensify. Additionally, when acetate is unidentate, the antisymmetric stretching peak broadens to 1590-1650 cm^{-1} [36]. This broadening is present for the 10,000 hour 'dark' specimen but not its 'light' counterpart. The 10,000 hour 'dark' sample shows elements of intermediate concentrations of acetate at the glass/EVA surface since the split peaks at ~1560 and ~1577 cm^{-1} are still evident (see inset of **Figure 4)** and of a moderate intensity with the ~1560 cm^{-1} peak providing the stronger signal. The 10,000 hour 'light' spectrum, however, reveals a merging of these peaks and significantly higher intensity, indicating an appreciably greater level of acetate. Increased concentrations under ‘light’ conditions would be expected since deacetylation is considerably accelerated by UV radiation [24]. As previously suggested, increased concentrations of species like these acetic salts at the glass/EVA interface could also contribute to the peak area loss of the ~2920 peak since they do not contain CH2 groups.

The buildup of acetic ions/salts at the glass/EVA interface implies a correlative buildup of acetic acid during aging. The increased concentration of acetic species at the glass/EVA interface has significant implications for autocatalyzing further deacetylation [37,38] and catalyzing other degradative reactions, which will be discussed later in 3.3. These FTIR-ATR data provide additional clarity regarding the specific degradation pathways occurring at the pertinent interfaces, and demonstrate that, in general, greater levels of degradation and reactivity occur at the glass/EVA interface with UV radiation intensifying the degradation.

Composition of constituent elements characterized with XPS at the glass/EVA and EVA/cell interfaces is reported for an unaged sample and for samples aged for 10,000 hours in ‘light’ and ‘dark’ conditions in **Figure 6**. Elemental compositions were obtained via analysis of associated survey scans (**Figure S1**). At the glass/EVA interface (**Figure 6a**), five elements were detected – carbon, oxygen, calcium, silicon, and sodium. No obvious trends exist between the unaged and aged specimen for the first four elements; however, sodium is absent initially but measurably increases after 10,000 hours in both ‘light’ and ‘dark’ conditions. At the EVA/cell interface (**Figure 6b**), only 4 elements were detected – carbon, oxygen, calcium, and silicon; sodium was not detected at any significant level even after aging.

XPS characterization confirms the existence of positive ions at the glass/EVA boundary, which facilitate acetate salt formation. The results suggest that a diffusion of sodium ions from the glass into the EVA occurs throughout the aging process. This sodium diffusion has been a consistent and well-documented element of potential induced degradation (PID) [39] and leads to the loss of desirable mechanical properties in EVA laminates [40] including the loss of adhesive strength [41], but these mini-modules were not connected to any voltage source during their exposures [42]. In this instance, a migration of sodium ions occurs under conditions of elevated temperature and moderate humidity without any voltage bias; still, even after 10,000 hours, these ions fail to penetrate through to the EVA/cell interface as seen in biased modules after just 1000 hours of accelerated conditions [41]. Calcium ions were present after initial lamination and remain present at similar levels throughout aging at the glass/EVA interface; however, the results indicate calcium along the EVA/cell interface only after aging. Most likely, the calcium signal arises from an additive like calcium stearate that is often included within polymer encapsulant formulations [43,44], and its less consistent detection arises from its low concentration.

3.3 Interdependencies of Degradation Pathways

This work also reveals a critical interdependency between the early deacetylation and the later hydrolytic depolymerization reactions. Predicting delamination requires an understanding of the breakdown of interfacial bonds. The primary interfacial bonds are made up of siloxanes, which result from the silane coupling agent incorporated into the EVA formulation. The silane interacts with both the organic polymer and the inorganic substrate (here, the silicon cell or front glass), greatly improving the adhesive strength [42,45]. Initially, the EVA/cell interface is weaker than the glass/EVA interface [18,46,47]; however, after significant exposure in UV conditions, this relationship inverts [16]. Results and analysis from the current study provide insight into the reasons behind this inversion.

Cypryk *et al.* conducted a robust theoretical study of the mechanism of acid-catalyzed Si-O bond cleavage specifically in siloxane bonds [48]. They confirmed that the neutral hydrolysis of siloxane bonds is extremely slow, which is consistent with experimental observations [48,49]. However, the energy barrier for hydrolysis at a neutral disiloxane molecule is ~500% greater than at a protonated disiloxane molecule. The significantly increased concentration of acetic species detected at the glass/EVA interface after 10,000 hours of exposure in 'light' conditions (see **Figure 5d**) suggests a highly acetic, and thus acidic, environment. Consequently, after significant exposure, the glass/EVA interface would experience accelerated hydrolysis reactions due to the buildup of acetic species. The mini-module exposed in 'dark' conditions saw a less substantial increase in the acetic peak. Fewer acetic species indicate a less acidic environment and would force the hydrolysis of siloxane bonds to propagate under more neutral conditions for longer, which, as stated before, is radically slower than in protonated conditions. The adhesion tests used to isolate the EVA on the same 10,000 hour mini-modules corroborate this assertion since only the 'light' sample preferentially failed at the glass/EVA interface. As discussed previously, FTIR-ATR results indicate greater overall levels of degradation, reactivity, and molecular network breakdown at the glass/EVA interface, even without considering UV exposure (see **Figure 5**). Altogether, these findings help explain why after years of exposure, delamination of the EVA preferentially occurs at the glass/EVA interface even though early adhesion studies repeatedly demonstrate that the EVA/cell interface is originally weaker. Furthermore, they clarify exactly why hydrolytic depolymerization becomes dominate and problematic at later time scales.

4. Conclusions

Through the analysis of EVA from mini-modules that underwent accelerated exposure to typical terrestrial stressors (elevated temperatures, humidity, and/or UV radiation), the critical degradation pathways for adhesive degradation of deacetylation, β-scission, and hydrolytic depolymerization were investigated and characterized after several lengths of exposure – up to 10,000 hours. This length of exposure allowed for a greater, controlled understanding of the effect these stressors have on EVA-based modules after potentially decades in the field. Advanced characterization techniques provided convincing evidence for these mechanisms' evolution as well as when they each tend to dominate the overall degradation. FTIR-ATR and XPS conducted at both interfaces isolated interface-specific effects, revealing that some degradation is nonuniform throughout the thickness of the EVA and greater levels of degradation are experienced at the glass/EVA interface.

Despite the limited crystallinity of EVA, GIWAXS detected changes in the relative proportions of crystalline phases after 10,000 hours of exposure in 'light' conditions, suggesting extensive β-scission reactions. DSC crystallinity results confirmed that deacetylation reactions tend to dominate initially before β-scission reactions take greater effect. Hydrolytic depolymerization has been understood to be a kinetically slow process; however, after extended periods of exposure, FTIR-ATR results from the glass/EVA interface revealed high levels of acetate salts, which heavily catalyze these hydrolysis reactions at the siloxane bonds. This explains how hydrolytic depolymerization, a kinetically limited process even in the presence of water, has the potential to become an increasingly dominate degradation mechanism after sufficient periods of UV exposure. This discovery highlights a critical interdependency between deacetylation and hydrolytic depolymerization, essential to holistically understanding adhesive degradation, and rationalizes why the critical failure interface transitions from EVA/cell to glass/EVA after significant exposure. Moreover, this work underscores the need for predictive, adhesive degradation models to account for degradation mechanism interdependencies if long-term accuracy is to be achieved.

Acknowledgments

This work was funded as part of the Durable Modules Materials Consortium (DuraMAT), an Energy Materials Network Consortium funded by the US Department of Energy, Office of Energy Efficiency and Renewable Energy, Solar Energy Technologies Office agreement number 32509. The views expressed in the article do not necessarily represent the views of the DOE or the US Government. The US Government retains and the publisher, by accepting the article for publication, acknowledges that the US Government retains a nonexclusive, paid-up, irrevocable, worldwide license to publish or reproduce the published form of this work, or allow others to do so, for US Government purposes. Use of the Stanford Synchrotron Radiation Lightsource, SLAC National Accelerator Laboratory, is supported by the U.S. Department of Energy, Office of Science, Office of Basic Energy Sciences under Contract No. DE-AC02-76SF00515. Part of this work was performed at the Stanford Nano Shared Facilities (SNSF), supported by the National Science Foundation under award ECCS-2026822. We would like to thank Dr. Kevin Stone at SLAC National Accelerator Laboratory for his valuable WAXS insights and Mike Kempe at NREL for his insight regarding estimation of acceleration factors.

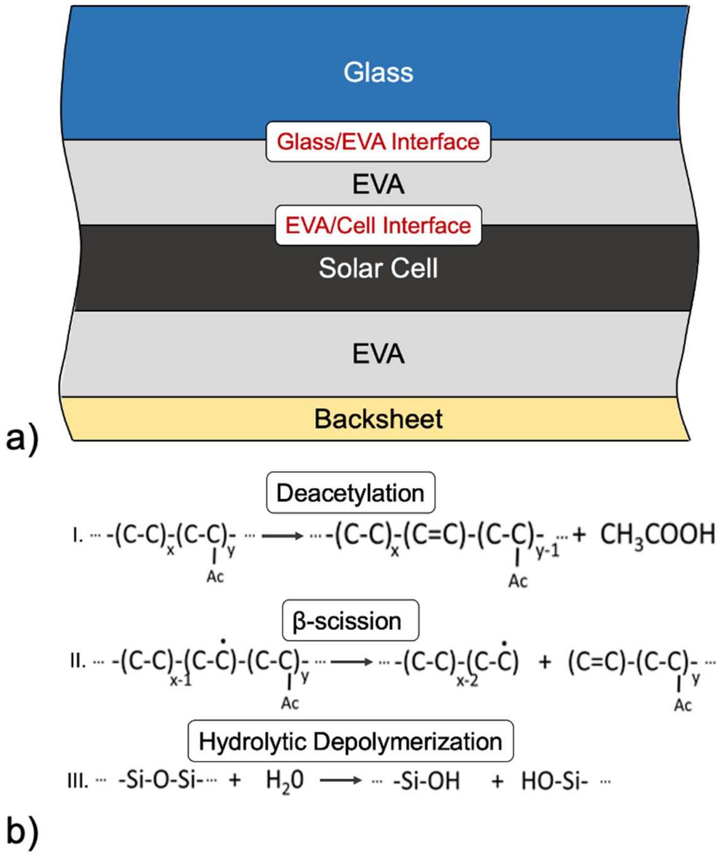

Figure 1: (a) Schematic illustration of the mini-modules and the relevant interfaces; (b) representative examples of encapsulant degradation mechanisms with corresponding reacting functional groups focusing on a polymer segment. For deacetylation, only one chemical reaction pathway is included. Repeat units are indicated by x and y with $y << x$. Ac indicates acetate group.

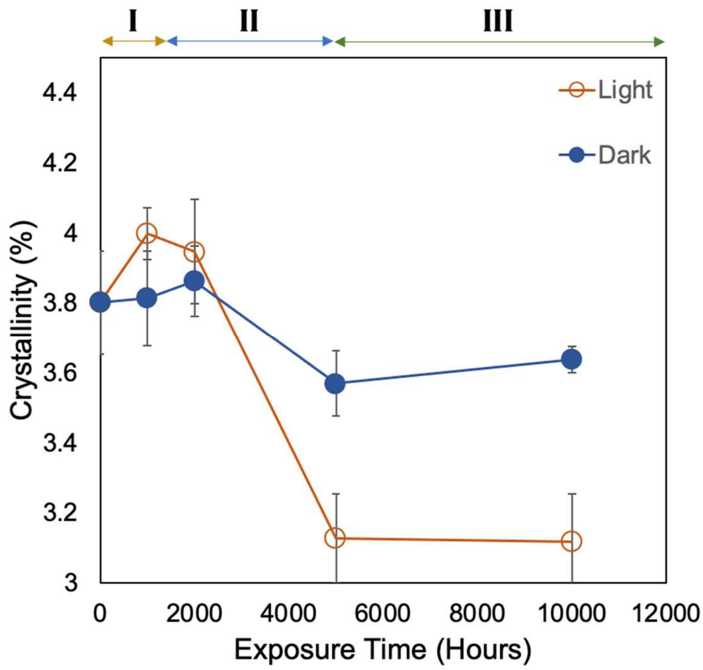

Figure 2: DSC analysis provides percent crystallinity of the EVA at several time points from 0 through 10,000 hours of accelerated aging. In 'light' conditions (orange, open), an initial increase in crystallinity is followed by a steep loss of crystallinity. In 'dark' conditions (blue, solid), a lesser increase initially occurs, which is followed by a minor decrease. The arrows above the figure indicate the approximate periods over which a given degradation mechanism – I, II, or III (see **Figure 1**) – dominates [18].

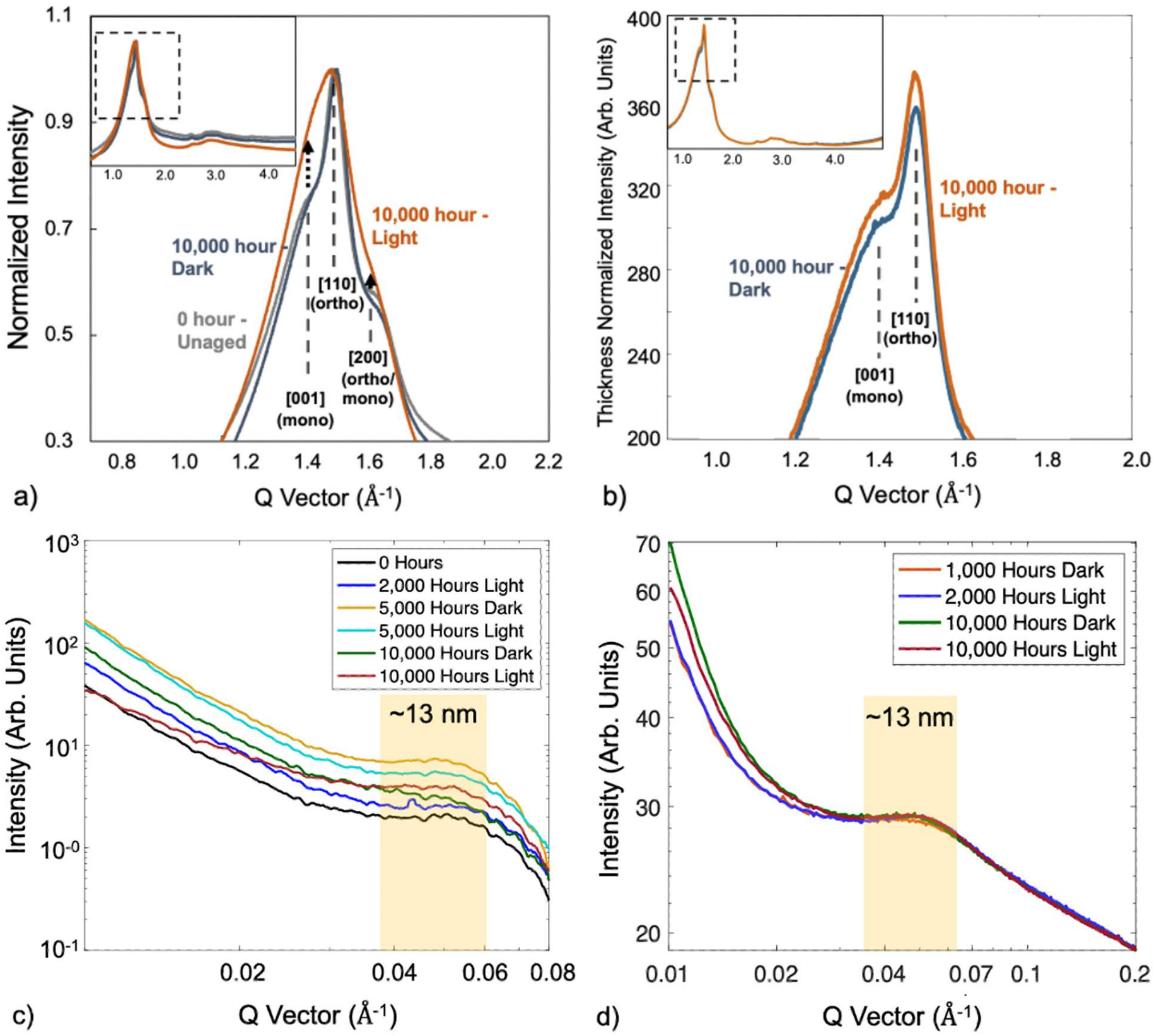

Figure 3: WAXS and SAXS were conducted in both grazing-incidence (a), (c) and transmission (b), (d) geometries on samples up through 10,000 hours of aging. Grazing-incidence WAXS results (a) reveal a change that occurs only under exposure to 'light' (orange) conditions. Transmission WAXS results (b) fail to reveal a similar shift. Both SAXS results (c), (d) highlight a characteristic spacing between amorphous and crystalline regions of ~13 nm.

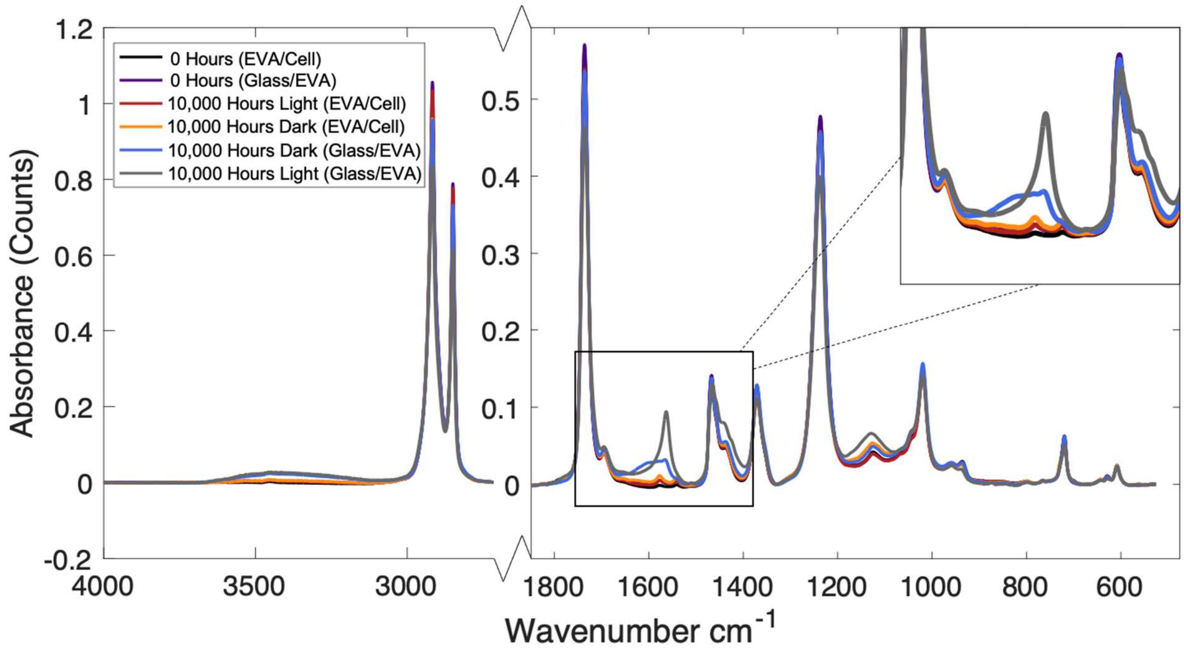

Figure 4: Several representative spectra from FTIR-ATR characterization along both the glass/EVA and EVA/cell interfaces before and after 10,000 hours of accelerated exposure are superimposed for visual comparison. Regions of interest involving peak changes and shifts are located near 3500, 2920, 1560, and 1125 cm^{-1}. More quantitative results are included in **Figure 5**.

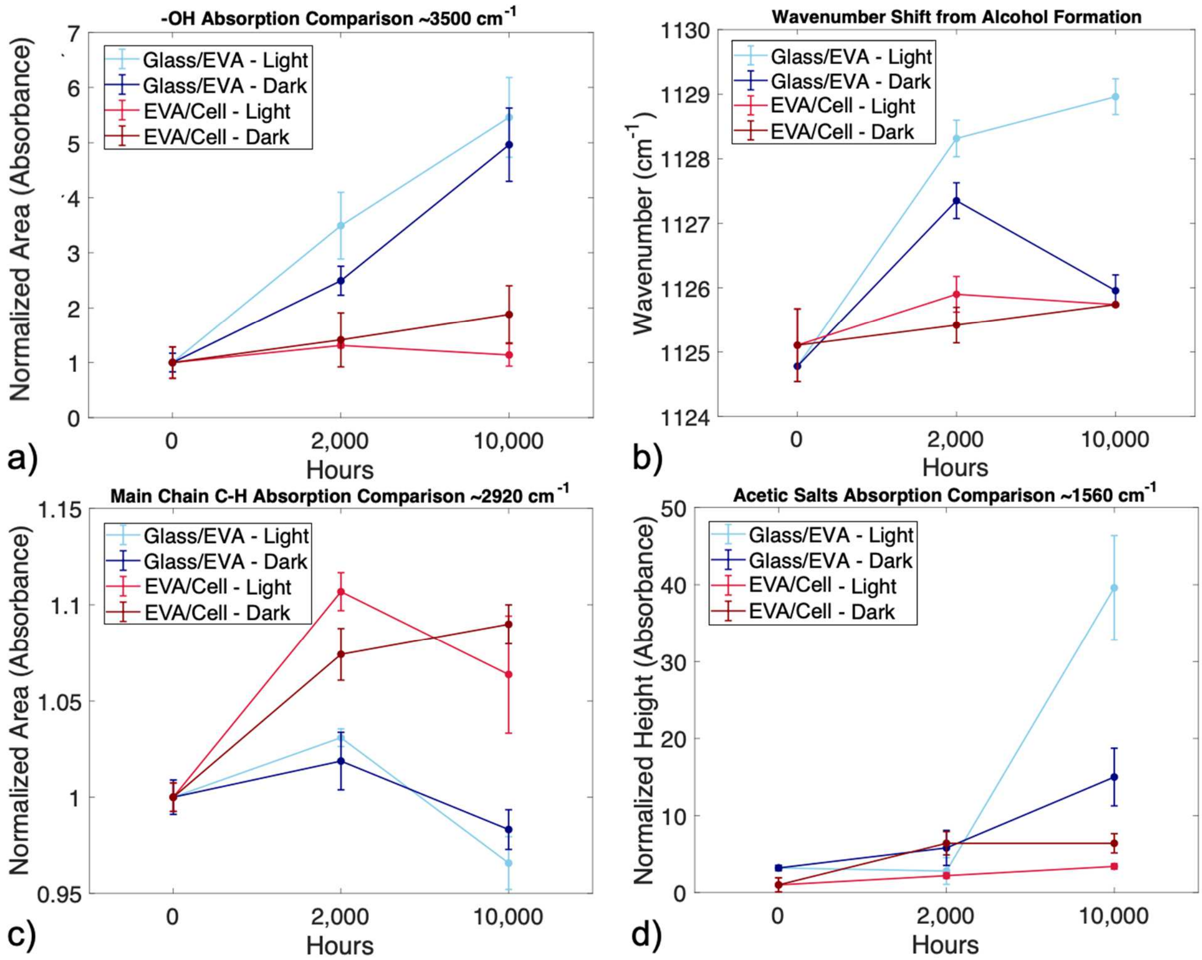

Figure 5: FTIR-ATR characterization along both the glass/EVA (light blue and dark blue) and EVA/cell (red and dark red) interfaces performed initially and after 2,000 and 10,000 hours of aging in 'dark' (dark blue and dark red) and 'light' (light blue and red) conditions. (a) reveals a substantial increase in –OH absorption along the glass interface. (b) presents the peak location for the secondary alcohol peak. (c) exhibits the divergent trend between the two interfaces at the ~2920 peak. (d) reveals the growth of acetic salts at the interfaces over the course of aging.

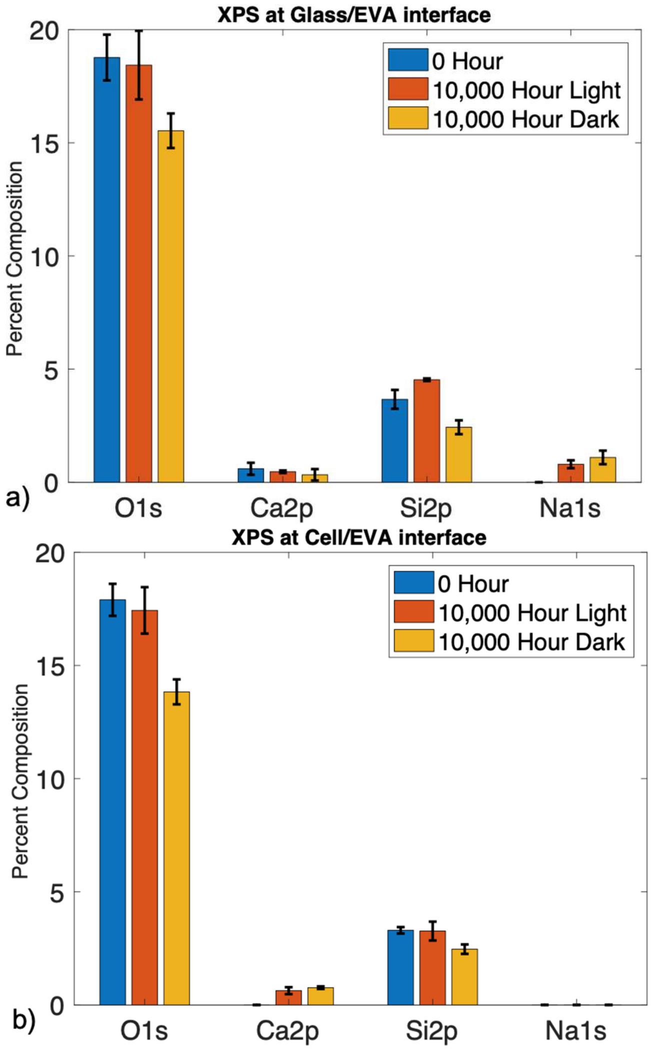

Figure 6: XPS characterization from both the glass/EVA (a) and the EVA/cell (b) interfaces. Sodium appears after 10,000 hours of aging only at the glass/EVA interface in both 'dark' and 'light' conditions. Note: Carbon (not included) makes up the remainder of each specimen's composition.

Bibliography

[1] A.W. Czanderna, F.J. Pern, Encapsulation of PV modules using ethylene vinyl acetate copolymer as a pottant: A critical review, Sol. Energy Mater. Sol. Cells. 43 (1996) 101–181. https://doi.org/10.1016/0927-0248(95)00150-6.

[2] A. El Amrani, A. Mahrane, F.Y. Moussa, Y. Boukennous, Solar Module Fabrication, Int. J. Photoenergy. 2007 (2007) 27610. https://doi.org/10.1155/2007/27610.

[3] M. Köntges, S. Kurtz, C.E. Packard, U. Jahn, K.A. Berger, K. Kato, T. Friesen, H. Liu, M. Van Iseghem, J. Wohlgemuth, D. Miller, M. Kempe, P. Hacke, F. Reil, N. Bogdanski, W. Herrmann, C. Buerhop-Lutz, G. Razongles, G. Friesen, Review of Failures of Photovoltaic Modules, (2014).

[4] M.L. Marín, A. Jiménez, J. López, J. Vilaplana, Thermal degradation of ethylene (vinyl acetate). Kinetic analysis of thermogravimetric data, J. Therm. Anal. 47 (1996) 247–258. https://doi.org/10.1007/BF01982703.

[5] B.-Å. Sultan, E. Sörvik, Thermal degradation of EVA and EBA—A comparison. I. Volatile decomposition products, J. Appl. Polym. Sci. 43 (1991) 1737–1745. https://doi.org/10.1002/app.1991.070430917.

[6] J. Jin, S. Chen, J. Zhang, UV aging behaviour of ethylene-vinyl acetate copolymers (EVA) with different vinyl acetate contents, Polym. Degrad. Stab. 95 (2010) 725–732. https://doi.org/10.1016/J.POLYMDEGRADSTAB.2010.02.020.

[7] A. Niemczyk, D. Moszyński, R. Jędrzejewski, K. Kwiatkowski, J. Piwowarczyk, J. Baranowska, Chemical structure of EVA films obtained by pulsed electron beam and pulse laser ablation, Polymers (Basel). 11 (2019). https://doi.org/10.3390/polym11091419.

[8] F.J. Pern, A.W. Czanderna, EVA degradation mechanisms simulating those in PV modules, in: AIP Conf. Proc., AIP Publishing, 2008: pp. 445–452. https://doi.org/10.1063/1.42901.

[9] K.E. Hrdina, J.W. Halloran, A. Oliveira, M. Kaviany, Chemistry of removal of ethylene vinyl acetate binders, J. Mater. Sci. 33 (1998) 2795–2803.

https://doi.org/10.1023/A:1017525501161.

[10] M. Çopuroğlu, M. Şen, A comparative study of thermal ageing characteristics of poly(ethylene-co-vinyl acetate) and poly(ethylene-co-vinyl acetate)/carbon black mixture, Polym. Adv. Technol. 15 (2004) 393–399. https://doi.org/10.1002/pat.485.

[11] G.A. Razuvaev, B.B. Troitskii, L. V. Chochlova, Z.B. Dubova, Thermal degradation of ethylene-vinyl acetate copolymer, J. Polym. Sci. Polym. Lett. Ed. 11 (1973) 521–523. https://doi.org/10.1002/pol.1973.130110805.

[12] D. Wu, J. Zhu, T.R. Betts, R. Gottschalg, PV Module Degradation Mechanisms under Different Environmental Stress Factors, Loughborough University, 2012. https://dspace.lboro.ac.uk/ (accessed September 14, 2020).

[13] A. Badiee, I.A. Ashcroft, R.D. Wildman, The thermo-mechanical degradation of ethylene vinyl acetate used as a solar panel adhesive and encapsulant, Int. J. Adhes. Adhes. 68 (2016) 212–218. https://doi.org/10.1016/j.ijadhadh.2016.03.008.

[14] D. Wu, J. Zhu, J. Frese, D. Montiel-Chicharro, T.R. Betts, R. Gottschalg, Effects of different lamination conditions on the reliability of encapsulation materials of pv modules: adhesion strength, in: 6th World Conf. Photovolt. Energy Convers., WCPEC-6, Kyoto, Japan, 2014. https://repository.lboro.ac.uk/articles/conference_contribution/Effects_of_different_lamination_conditions_on_the_reliability_of_encapsulation_materials_of_pv_modules_adhesion_strength/9557159 (accessed September 14, 2020).

[15] A. Badiee, R. Wildman, I. Ashcroft, Effect of UV aging on degradation of Ethylene-vinyl Acetate (EVA) as encapsulant in photovoltaic (PV) modules, in: N.G. Dhere, J.H. Wohlgemuth, R. Jones-Albertus (Eds.), Reliab. Photovolt. Cells, Modul. Components, Syst. VII, SPIE, 2014: p. 91790O. https://doi.org/10.1117/12.2062007.

[16] N. Bosco, J. Tracy, R. Dauskardt, S. Kurtz, Development and first results of the width-tapered beam method for adhesion testing of photovoltaic material systems, in: Conf. Rec. IEEE Photovolt. Spec. Conf., Institute of Electrical and Electronics Engineers Inc., 2016: pp. 106–110. https://doi.org/10.1109/PVSC.2016.7749558.

[17] J. Tracy, N. Bosco, F. Novoa, R. Dauskardt, Encapsulation and backsheet adhesion metrology for photovoltaic modules, Prog. Photovoltaics Res. Appl. 25 (2017) 87–96. https://doi.org/10.1002/pip.2817.

[18] J. Tracy, D.R. D'hooge, N. Bosco, C. Delgado, R. Dauskardt, Evaluating and predicting molecular mechanisms of adhesive degradation during field and accelerated aging of photovoltaic modules, Prog. Photovoltaics Res. Appl. 26 (2018) 981–993. https://doi.org/10.1002/pip.3045.

[19] N. Bosco, J. Eafanti, S. Kurtz, J. Tracy, R. Dauskardt, Defining Threshold Values of Encapsulant and Backsheet Adhesion for PV Module Reliability, IEEE J. Photovoltaics. 7 (2017) 1536–1540. https://doi.org/10.1109/JPHOTOV.2017.2746682.

[20] B.H. Toby, R.B. Von Dreele, GSAS-II: The genesis of a modern open-source all purpose crystallography software package, J. Appl. Crystallogr. 46 (2013) 544–549. https://doi.org/10.1107/S0021889813003531.

[21] J. Ilavsky, Nika: Software for two-dimensional data reduction, J. Appl. Crystallogr. 45 (2012) 324–328. https://doi.org/10.1107/S0021889812004037.

[22] W. Hu, E.B. Sirota, Monoclinic Crystallites in Ethylene Copolymers Detected by Solid-State NMR and X-ray Diffraction, Macromolecules. 36 (2003) 5144–5149. https://doi.org/10.1021/ma030132n.

[23] T. Meier, C. Peike, T. Kaltenbach, K.-A. Weiß, Changes of morphology and material properties of thin ethylene-vinyl acetate-films under different aging conditions, in: 28th Eur. PV Sol. Energy Conf. Exhib., Paris, France, 2013.

[24] X. Gu, C.-C. Lin, S. Ogier, Y. Pang, K.-T. Tan, K. Connolly, P. Krommenhoek, J. Chin, Accelerated Laboratory Testing of PV Polymers using Simultaneous UV Radiation, Temperature and Moisture, Gaithersburg, MD, 2013. https://www.nist.gov/system/files/documents/el/building_materials/Gu.pdf.

[25] J.C. Schlothauer, K. Grabmayer, I. Hintersteiner, G.M. Wallner, B. Röder, Non-destructive 2D-luminescence detection of EVA in aged PV modules: Correlation to

calorimetric properties, additive distribution and a clue to aging parameters, Sol. Energy Mater. Sol. Cells. 159 (2017) 307–317. https://doi.org/10.1016/J.SOLMAT.2016.09.011.

[26] R.J. Herling, ed., Durability Testing of Nonmetallic Materials, West Conshohocken, PA, 1996. https://doi.org/10.1520/STP1294-EB.

[27] Coblentz Society Inc., Evaluated Infrared Reference Spectra, in: P.J. Linstrom, W.G. Mallard (Eds.), NIST Chem. WebBook, NIST Stand. Ref. Database Number 69, National Institute of Standards and Technology, Gaithersburg, MD, n.d. https://doi.org/https://doi.org/10.18434/T4D303.

[28] IR Spectrum Table & Chart | Sigma-Aldrich, (n.d.). https://www.sigmaaldrich.com/technical-documents/articles/biology/ir-spectrum-table.html (accessed February 10, 2020).

[29] R.C. Petersen, J.H. Wohlgemuth, Stability of EVA modules, in: Conf. Rec. IEEE Photovolt. Spec. Conf., Publ by IEEE, 1992: pp. 562–565. https://doi.org/10.1109/pvsc.1991.169276.

[30] U. Weber, R. Eiden, C. Strubel, T. Soegding, M. Heiss, P. Zachmann, K. Nattermann, H. Engelmann, A. Dethlefsen, N. Lenck, Acetic acid production, migration and corrosion effects in ethylene-vinyl- acetate- (EVA-) based pv modules, 27th Eur. Photovolt. Sol. Energy Conf. Exhib. (2012) 2992–2995. https://doi.org/10.4229/27thEUPVSEC2012-4CO.9.4.

[31] L.W. Tang, K.C. Tam, C.Y. Yue, X. Hu, Y.C. Lam, L. Li, Morphology and mechanical properties of reactive compatibilized polystyrene/ethylene-vinyl acetate-vinyl alcohol blends, J. Appl. Polym. Sci. 85 (2002) 209–217. https://doi.org/10.1002/app.10627.

[32] R.J. Koopmans, E.F. Vansant, R. Van Der Linden, The Characterisation of Newly Developed and Promising Hydrolyzed Ethylene Vinyl Acetate Copolymers, J. Adhes. 11 (1980) 191–202. https://doi.org/10.1080/00218468008078916.

[33] E. Hagting, An investigation on the effect of clusters in thermo-reversible cross-linked rubbers, University of Groningen, 2015. http://fse.studenttheses.ub.rug.nl/13628/.

[34] W. Holley, S.C. Agro, Advanced EVA-Based Encapsulants, Final Report January 1993-June 1997, 1998. https://doi.org/NREL/SR-520-25296.

[35] M. Köntges, G. Oreski, U. Jahn, M. Herz, P. Hacke, K.-A. Weiss, G. Razongles, M. Paggi, D. Parlevliet, T. Tanahashi, R.H. French, Assessment of Photovoltaic Module Failures in the Field, (2017).

[36] A.Q. Wang, T.D. Golden, Electrodeposition of Oriented Cerium Oxide Films, Int. J. Electrochem. 2013 (2013) 482187. https://doi.org/10.1155/2013/482187.

[37] B.B. Troitskii, G.A. Razuvaev, L. V. Khokhlova, G.N. Bortnikov, On the mechanism of the thermal degradation of polyvinyl acetate, J. Polym. Sci. Polym. Symp. 42 (2007) 1363–1375. https://doi.org/10.1002/polc.5070420336.

[38] J.M. Barrales-Rienda, M. Sánchez Chaves, J.M. Mazón Arechederra, F. Fernández Martín, Polymer precursors of polyacetylene. Thermal degradation of poly(vinyl esters). Part 1-Molecular weight dependence of the autocatalytic thermal degradation of poly(vinyl acetate) (PVAc), Polym. Degrad. Stab. 21 (1988) 55–72. https://doi.org/10.1016/0141-3910(88)90065-1.

[39] M. Kempe, Encapsulant Materials for PV Modules, in: Photovolt. Sol. Energy, John Wiley & Sons, Ltd, Chichester, UK, 2017: pp. 478–490. https://doi.org/10.1002/9781118927496.ch43.

[40] N.G. Dhere, Reliability of PV modules and balance-of-system components, in: Conf. Rec. Thirty-First IEEE Photovolt. Spec. Conf. 2005., 2005: pp. 1570–1576. https://doi.org/10.1109/PVSC.2005.1488445.

[41] N. Bosco, S. Moffitt, L.T. Schelhas, Mechanisms of adhesion degradation at the photovoltiac module's cell metallization-encapsulant interface, Prog. Photovoltaics Res. Appl. 27 (2019) 340–345. https://doi.org/10.1002/pip.3106.

[42] F.J. Pern, G.J. Jorgensen, Enhanced Adhesion of EVA Laminates to Primed Glass Substrates Subjected to Damp Heat Exposure, 2005. http://www.osti.gov/bridge (accessed May 29, 2020).

[43] COAD ® 13 CALCIUM STEARATE SERIES POLYOLEFIN APPLICATIONS: TYPICAL PROPERTIES COAD ® 13 D COAD ® 13F COAD ® 13M, (n.d.).

[44] F. Gaston, N. Dupuy, S.R.A. Marque, D. Gigmes, S. Dorey, Monitoring of the discoloration on γ-irradiated PE and EVA films to evaluate antioxidant stability, J. Appl. Polym. Sci. 135 (2018) 46114. https://doi.org/10.1002/APP.46114.

[45] J.L. Koenig, F.J. Boerio, E.P. Plueddemann, J. Miller, P.B. Willis, E.F. Cuddihy, Flat-Plate Solar Distribution Category UC-63b Array Project Chemical Bonding Technology: Direct Investigation of Interfacial Bonds, n.d. https://ntrs.nasa.gov/search.jsp?R=19860012113 (accessed May 29, 2020).

[46] J. Wohlgemuth, T. Silverman, D.C. Miller, P. McNutt, M. Kempe, M. Deceglie, Evaluation of PV module field performance, in: 2015 IEEE 42nd Photovolt. Spec. Conf. PVSC 2015, Institute of Electrical and Electronics Engineers Inc., 2015. https://doi.org/10.1109/PVSC.2015.7356132.

[47] J. Tracy, N. Bosco, C. Delgado, R. Dauskardt, Durability of ionomer encapsulants in photovoltaic modules, Sol. Energy Mater. Sol. Cells. 208 (2020) 110397. https://doi.org/10.1016/j.solmat.2020.110397.

[48] M. Cypryk, Y. Apeloig, Mechanism of the Acid-Catalyzed Si−O Bond Cleavage in Siloxanes and Siloxanols. A Theoretical Study, Organometallics. 21 (2002) 2165–2175. https://doi.org/10.1021/om011055s.

[49] J. Chojnowski, in Silicon-containing polymers, Royal Society of Chemistry, Cambridge, 1995.